MULTIYEAR SIMULATIONS OF THE MARTIAN WATER CYCLE WITH THE AMES GENERAL CIRCULATION MODEL. S. M. Nelli[1,*], J. R. Murphy[1], R. M. Haberle[2], and J. R. Schaeffer[2], [1]Department of Astronomy, New Mexico State University, P.O. Box 30001/MSC 4500, 1320 Frenger Street, Las Cruces, NM 88003-8001, USA. [*]e-mail address: snelli@nmsu.edu (S. M. Nelli), [2]NASA-Ames Research Center, Moffett Field, CA 94035, USA.

Introduction: Mars' atmosphere is carbon dioxide dominated with non-negligible amounts of water vapor and suspended dust particles. The atmospheric dust plays an important role in the heating and cooling of the planet through absorption and emission of radiation. Small dust particles can potentially be carried to great altitudes and affect the temperatures there. Water vapor condensing onto the dust grains can affect the radiative properties of both, as well as their vertical extent. The condensation of water onto a dust grain will change the grain's fall speed and diminish the possibility of dust obtaining high altitudes. In this capacity, water becomes a controlling agent with regard to the vertical distribution of dust. Similarly, the atmosphere's water vapor holding capacity is affected by the amount of dust in the atmosphere. Dust is an excellent green house catalyst; it raises the temperature of the atmosphere, and thus, its water vapor holding capacity. There is, therefore, a potentially significant interplay between the Martian dust and water cycles.

Previous research done using global, 3-D computer modeling to better understand the Martian atmosphere treat the dust and the water cycles as two separate and independent processes [1]. The existing Ames numerical model will be employed to simulate the relationship between the Martian dust and water cycles by actually coupling the two cycles. Water will condense onto the dust, allowing the particle's radiative characteristics, fall speeds, and as a result, their vertical distribution to change. Data obtained from the Viking, Mars Pathfinder, and especially the Mars Global Surveyor missions will be used to determine the accuracy of the model results.

General Circulation Model: The water and dust cycles in the model will be coupled by depositing supersaturated water vapor onto the dust grains to form ice clouds. By using the dust as seeds for cloud formation, the radiative properties, fall speeds and vertical distributions of both will be altered [2,3,4]. Water ice encapsulating the dust grains makes the dust much less effective at the 15µm absorption band, but increases their potential as infrared scatterers [4]. Mie scattering (the scattering of light by a particle whose size is comparable to the wavelength of light) becomes important with the formation of cloud particles a few microns in size. The effectiveness of Mie scattering is large when the size parameter is $2\pi r/\lambda \geq 1$, where r is the radius of the particle and λ is the wavelength of light.

The addition of water mass to these dust grains influences the gravitational sedimentation speed. Initially, the increase in mass decreases the sedimentation speed, and then the fall speed rapidly increases once the particle has doubled in radius, removing dust more quickly from the atmosphere [5]. The vertical extent of the dust will be at the mercy of the cloud deck. Little, if any, dust will be able to be transported past the saturation layer. Here, the dust will be used for seeds in cloud formation, effectively capping its altitude. The "snowing out" of these particles will move water out of the saturated layer to lower vertical levels as well.

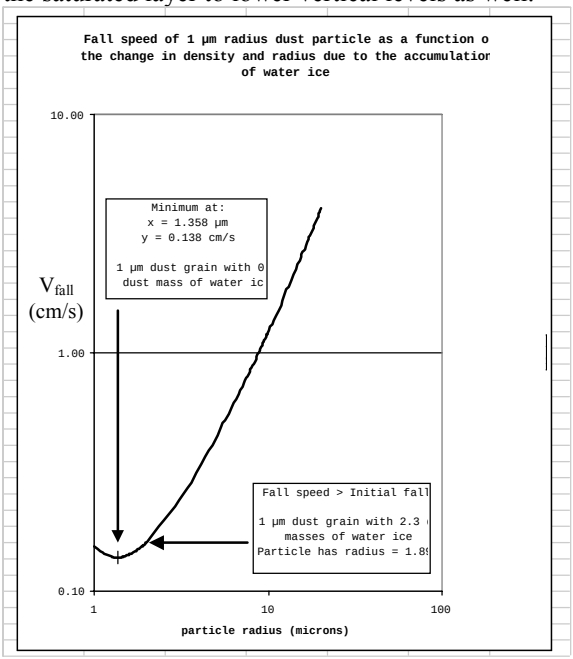

Figure 1. Fall speed vs. particle radius for a 1µm dust grain accumulating water ice. Initially, fall speed decreases since the decrease in density is the dominating factor. This trend is quickly reversed, as size (radius) of the particle becomes more dominant. The formulation of this curve is based on that found in [5].

Sublimation of ground ice is based upon the flux rate equations of Haberle and Jakosky [6] for buoyant diffusion (E_b) and turbulent mixing (E_t). These two processes are as follows:

$$E_b = (0.17)(\delta\eta)\rho D[(\delta\rho/\rho)(g/v^2)]^{1/3}$$

and

$$E_t = (0.002)\rho w q_s(1 - r)$$

where δη is the difference between the surface concentration (by mass) of water vapor and that of the gas away from the surface, ρ is the density of the atmosphere, D is the diffusion coefficient of water vapor in CO_2, g is the acceleration due to gravity, ν is the kinematic viscosity of CO_2, δρ is the difference between the density of the atmosphere at the surface and the density of water vapor at the surface, *w* is the wind speed at the surface layer, q_s is the saturation mixing ratio of water vapor at the temperature of the ice, and r is the relative humidity [6].

The model will contain an adsorbing regolith based on the scheme developed by Houben et al. [7]. Water will be mobilized in an approximately 10 cm thick ground layer. The total adsorbed water capacity is by:

$$\alpha = \varepsilon\rho_s[\beta P^{0.51}{}_{H2O}/\exp(\delta/T)]$$

where ρ_s is the density of the regolith, β is the specific soil surface area for basalt, δ = -2679.8 K, T is the temperature, P_{H2O} is the water vapor pressure in Pascals, and ε is a dimensionless parameter introduced to allow for scaling the adsorptive properties of other minerals. Increasing the value of ε will increase the adsorptivity of the soil, meaning the regolith can hold more water per unit volume [7].

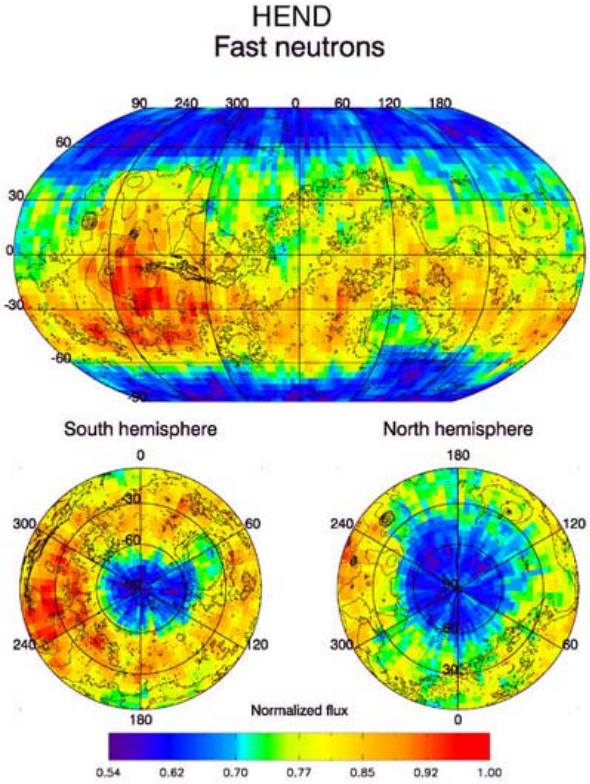

Figure 2. Initial map of fast neutrons by the High Energy Neutron Detector (HEND) on Mars Odyssey. Red areas are hydrogen-poor soil, while blue areas are hydrogen-rich. Note that Solis Planum (270˚E, 30˚S) is the most hydrogen-poor region on the planet. Hydrogen-rich areas extend from both poles to approximately 60˚ latitude, probably water ice buried beneath hydrogen-poor soil. Also, two smaller regions of hydrogen-rich soil occur in the equatorial zone, probably subsurface deposits of chemically and/or physically bound H_20 and OH. One is located at approximately 30˚ E and the other at 200˚ E longitude [8,10]. Figure by Mitrofanov et al. 2002.

The Mars Odyssey Orbiter is carrying a suite of instruments known as the Gamma Ray Spectrometer (GRS). The Martian water content in the top meter of soil can be determined independently by two instruments of the GRS suite [9]. A gamma ray spectrometer aboard GRS can directly measure the emission of hydrogen gamma rays. These gamma rays are detectable from the upper tens of centimeters in the surface [9]. A neutron spectrometer aboard GRS can indirectly sample hydrogen in the upper meter of the surface [9,10]. Since 99.985% of all hydrogen is in the form of ^1H (no neutrons), then hydrogen is detected by its characteristic lack of neutron production by cosmic rays. Comparison of these two independent results will allow a determination of the water distribution as a function of surface depth (maximum depth of ~1 meter) [9,10].

The current model will have an active regolith of only ~10 cm deep. GRS will help to constrain this model regolith since the GRS can obtain a vertical distribution for the adsorbed water of ~1 m, which is greater than that included into the model (~10 cm). Odyssey data will be used to tune the important parameter of water distribution in the upper one meter of the regolith.

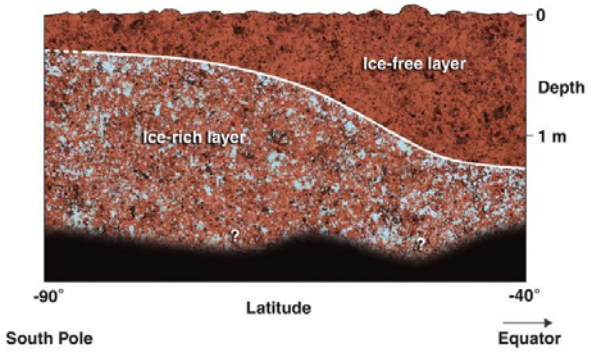

Figure 3. The Gamma Ray Spectrometer can determine the vertical distribution of ground water ice down to ~1 meter in depth. The above diagram is one possible configuration for water ice in the Martian regolith. Initial measurements suggest that the topmost layer of regolith is relatively ice-free. While a few tens of centimeters down, the regolith is 20 to 50 percent water ice by mass [11].

Figure taken from the web page of http://www.jpl.nasa.gov/images/mars/pia3803_caption.html

Discussion: TES and MAWD data will be looked at extensively to tune the model. Both TES and MAWD data will be used to help identify other possible sources and sinks of water vapor besides the north polar cap. TES will also be influential in identifying sources of dust storm activity by direct observation of where they begin, as well as finding possible sinks by identifying changes in surface albedo as a result of dust storm activity. GRS will be used to identify heterogeneity in the regolith, which previous models described homogeneously [1,7].

Smith (2001) compares the TES and MAWD data sets for the water vapor column abundance and finds three key differences [12]. At low northern latitudes between Ls = 150˚ and 205˚, TES retrieves water vapor abundances 20-40% higher than that of MAWD. TES sees a gradual increase in water vapor abundance between Ls = 40˚ and 90˚ at mid-northern latitudes, where as MAWD sees an abrupt increase between Ls = 60˚ and 75˚. Finally, excluding the dusty period of Ls = 205˚-330˚ seen by MAWD, TES derives a globally averaged amount of water vapor 10-20% higher than that seen by MAWD. These three differences are all within the error bars of the two instruments, but may be explained by interannual variability [12]. Coupling of the dust and water cycles in the model and running a multiyear simulation may help to disentangle the reason behind the differences in the TES and MAWD data sets.

The objective of this project is to determine the role the water cycle plays in interannual variability of the Martian atmosphere when coupled with the dust cycle. A possible consequence of the decoupling of the two cycles is that previous long duration models show no yearly variations. The patterns of dust lifting and sedimentation remain the same throughout multiple-year runs [13].

We are currently implementing the above mentioned water physics into the latest version of the Ames GCM. We will run the full 3-D model with just a polar source to be used as a base comparison. Subsequently, a multiyear run with an active regolith based on initial Mars Odyssey findings will be performed.

Acknowledgements: This work is being supported by NASA's Planetary Atmospheres Program (NASA/NAG5–1213) and also by the New Mexico Space Grant Consortium.

References: [1] Richardson R. I. and Wilson R. J. (2002) *JGR, 107*, 7-1–7-31. [2] Rodin A. V. et al. (1999) *Advances in Space Science*, *23*, 1577-1585. [3] Clancy R. T. et al. (1996) *Icarus, 122*, 36-62. [4] Clancy R. T. et al. (1998) *AAS, DPS meeting #30*, Abstract #09.02. [5] Murphy et al. (1990) *JGR*, *95*, 14629-14648. [6] Haberle R.M. and Jakosky B.M. (1990) *JGR*, *95*, 1423-1437. [7] Houben H. et al. (1997) *JGR*, *102*, 9069-9083. [8] Mitrofanov I. et al. (2002) *Science, 297*, 78-81. [9] Boyton W. V. et al. (2002) *Science, 297*, 81-85. [10] Feldman W. C. et al. (2002) *Science, 297*, 75-78. [11] http://www.jpl.nasa.gov/images/mars/pia3803_caption.html [12] Smith M. D. (2002) *JGR, 107*, 25-1. [13] Murphy J. R. (1999) *5th International Conference on Mars*, Abstract #6087.